Ultrafast Photovoltaic Response in Ferroelectric Nanolayers

Dan Daranciang[1,2], Matthew J. Highland[3], Haidan Wen[4], Steve M. Young[5], Nathaniel C. Brandt[6], Harold Y. Hwang[6], Michael Vattilana[7], Matthieu Nicoul[7], Florian Quirin[7], John Goodfellow[8,9], Tingting Qi[5], Ilya Grinberg[5], David M. Fritz[10], Marco Cammarata[10], Diling Zhu[10], Henrik T. Lemke[10,11], Donald A. Walko[4], Eric M. Dufresne[4], Yuelin Li[4], Jörgen Larsson[12], David A. Reis[2,9,13], Klaus Sokolowski-Tinten[7], Keith A. Nelson[6], Andrew M. Rappe[5], Paul H. Fuoss[3], G. Brian Stephenson[3] and Aaron M. Lindenberg[2,8,9]*

[1]*Department of Chemistry, Stanford University, Stanford, CA 94305*

[2]*PULSE Institute for Ultrafast Energy Science, SLAC National Accelerator Laboratory, Menlo Park, CA 94025*

[3]*Materials Science Division, Argonne National Laboratory, Argonne, IL 60439*

[4]*Advanced Photon Source, Argonne National Laboratory, Argonne, IL 60439*

[5]*The Makineni Theoretical Laboratories, Department of Chemistry, University of Pennsylvania, Philadelphia, PA 19104*

[6]*Department of Chemistry, Massachusetts Institute of Technology, Cambridge, MA 02139*

[7]*Faculty of Physics and Center for Nanointegration Duisburg-Essen (CeNIDE), University of Duisburg-Essen, 47048 Duisburg, Germany*

[8]*Department of Materials Science and Engineering, Stanford University, Stanford, CA 94305*

[9]*Stanford Institute for Materials and Energy Science, SLAC National Accelerator Laboratory, Menlo Park, CA 94025*

[10]*Linac Coherent Light Source, SLAC National Accelerator Laboratory, Menlo Park, CA 94025*

[11]*Niels Bohr Institute, University of Copenhagen, 2100 Copenhagen, Denmark*

[12]*Department of Physics, Lund University, S-22100 Lund, Sweden*

[13]*Department of Applied Physics, Stanford University, Stanford, CA 94305*

*e-mail: aaronl@stanford.edu

Work supported in part by US Department of Energy contract DE-AC02-76SF00515.

Abstract

We show that light drives large-amplitude structural changes in thin films of the prototypical ferroelectric PbTiO3 via direct coupling to its intrinsic photovoltaic response. Using time-resolved x-ray scattering to visualize atomic displacements on femtosecond timescales, photoinduced changes in the unit-cell tetragonality are observed. These are driven by the motion of photogenerated free charges within the ferroelectric and can be simply explained by a model including both shift and screening currents, associated with the displacement of electrons first antiparallel to and then parallel to the ferroelectric polarization direction.

Text

Light couples to atomic-scale degrees of freedom in complex materials, offering new avenues for engineering functionality in nanoelectronic devices and enhancing material properties. The key functionality of ferroelectrics—a thermodynamically stable, switchable polarization that persists even in the absence of an applied electric field—itself destabilizes the ferroelectric phase in thin films, due to the existence of an internal depolarization field [1-7], associated with the surface charge density $\sigma = \mathbf{P} \cdot \mathbf{n}$ (where **P** is the electric polarization and **n** is the unit normal vector), that points opposite to the direction of the polarization. This field can be screened by surface adsorbates or free charges [1,5], as in the simple case of ferroelectric capacitors with metallic electrodes, and can lead to the formation of stripe domains: periodic nanometer-scale domains of alternating polarization that minimize the free energy of the system [3,4,8]. Intensive research has been aimed at bypassing the intrinsic size limits imposed by the depolarization field on the ferroelectric phase, including epitaxial strain engineering [2,9,10] and the use of electrodes to screen the depolarization field [6,11].

At the same time, ongoing work over several decades [12-21] has sought to elucidate photovoltaic effects in ferroelectrics and multiferroics and the role of the depolarization field in these phenomena [15,19]. These are associated with the splitting of electron-hole pairs within a noncentrosymmetric crystal and lead to the generation of open-circuit voltages much larger than the bandgap. A number of mechanisms have been implicated in these effects, including the presence of the internal depolarization field in thin films [15], internal fields at domain walls [18], and second-order nonlinear optical responses in the field of the incident light in the

medium [21,22]. Such nonlinear responses include (non-resonant) optical rectification [21]; shift currents (also referred to as the "linear photovoltaic effect" [22]), associated with an anisotropic displacement of electrons and holes; and injection currents [22]. Little is known about the coupling of these photogenerated currents to the structural response of ferroelectrics. In addition, the possibility of using light to drive structural changes has been of continuing interest [23-27]. Previous time-resolved x-ray studies have focused on ferroelectric heterostructures, in which photons are absorbed within metallic layers in order to launch acoustic strain responses within the ferroelectric [27]. Here, using femtosecond time-resolved x-ray scattering, we report changes in tetragonality lasting several nanoseconds in the prototypical ferroelectric perovskite $PbTiO_3$ (PTO), following photoexcitation by ultrafast 400 nm light pulses. This result can be understood by taking into account the coupling of the photogenerated, time-dependent internal fields to the strain within the film.

We performed femtosecond time-resolved x-ray diffraction measurements of a 20 nm PTO film on $SrTiO_3$ (STO) and a 100 nm PTO film on $DyScO_3$ (DSO), without intermediary electrodes, in air, under photoexcitation by ultrafast 400 nm laser pulses. Due to the differing in-plane strains provided by STO (001) and the pseudocubic DSO (110) face, T_C of the two films is 680° C and 470° C, respectively [9]. We studied PTO on DSO in order to access states above T_C while avoiding the decomposition of the film at high temperature due to loss of volatile PbO [8]. Femtosecond 400 nm laser pulses were generated via second-harmonic generation from 800 nm, 40 fs full width at half max (FWHM) Ti:sapphire laser pulses and incident upon the samples with *s*-polarization at a 60° angle from the normal, with a maximum incident fluence of 5 mJ/cm^2 (≈ 100 GW/cm^2). X-ray pulses with 60 fs FWHM [28] and λ□= 1.39Å were scattered from the films after being monochromatized in a Si (111) double-crystal monochromator at the Linac Coherent Light Source, giving ~10^{10} photons/pulse incident on the sample at a 60 Hz repetition rate. We observed no evidence of x-ray-induced sample modification. The time resolution of this measurement is limited by timing jitter between laser and x-ray pulses, estimated to be 100 fs RMS [29]. The PTO (003) Bragg reflection was collected with either a point detector or an area detector as a function of laser delay and x-ray incidence angle (θ), probing the out-of-plane lattice parameter, *c*, inside the thin film. Similar experiments were performed at the Advanced Photon Source, but temporal resolution was limited to 100 ps by the synchrotron x-ray

pulse duration. Thin films of PTO were deposited on STO (001) and DSO (110) substrates at 930-990 K via metal-organic chemical vapor deposition, following procedures described elsewhere [30]. Prior to growth, TiO_2-terminated surfaces of STO were created via a standard HF etch [31]. DSO surfaces were prepared with ScO_2 termination by annealing in O_2, followed by a NaOH etch [32].

When grown on STO (001), PTO forms out-of-plane, *c*-axis-oriented domains below the Curie temperature, T_C, due to compressive strain from lattice mismatch to the STO [2,3,9]. Under zero-field heating conditions, the *c*-axis of PTO contracts as T_C is approached, corresponding to a negative thermal expansion coefficient. This contraction indicates a decrease in the tetragonality and the dipole moment of the unit cell, and causes out-of-plane diffraction peaks to shift to higher scattering angles. In contrast to the expected thermally induced responses, we observe significantly more complex dynamics. Time-dependent rocking curves of photoexcited, monodomain PTO on STO, with polarization pointing out of the film [33], taken at room temperature [Fig. 1(a) and Fig. 1(b)] indicate a symmetric shift of the Bragg peak to higher Q [where $Q = (4\pi \sin\theta)/\lambda$] within 5 ps. This is consistent with a uniform contraction of the unit cell in the out-of-plane direction and occurs on an acoustically limited timescale, determined by the film thickness over the sound velocity ($v_s \approx 4{,}000$ m/s) [34]. Subsequently, we observe a long-lived, symmetric shift of the diffraction peak to lower Q occurring on a 10 ps timescale, in contrast to what would be expected from simple heating of a ferroelectric. Following the low-Q shift, the nanolayer relaxes to its initial state before excitation on single-nanosecond timescales [Fig. 1(c)]. We note that the in-plane lattice constants are expected to evolve on acoustically limited timescales determined by the 1-mm laser spot size, and therefore do not change on the picosecond timescales here.

In order to further elucidate the time-dependent changes in the ferroelectric unit cell, we measured the response of the system at 535° C, where PTO on STO enters a stripe domain phase [3], characterized by neighboring regions of opposite polarization, with a period Λ of order 10 nm. This period is determined by a trade-off between the energy of the uncompensated depolarization field and the domain walls [8]. At higher temperatures, the volatile adsorbate species that stabilize the monodomain phase [1,5] are removed. The periodicity of the stripe domains gives rise to in-plane satellites, displaced by $\Delta Q_r = 2\pi/\Lambda$, which appear as a ring of

diffuse scattering around the Bragg peak. We measured the time evolution of this diffuse scattering under photoexcitation (Fig. 2). After correcting the orientation of the imaging plane to make it normal to the *L*-axis in reciprocal space [Fig. 2(a)], the distance in reciprocal space from the Bragg peak to the center of the diffuse scattering was defined to be $Q_r = (Q_H^2 + Q_K^2)^{1/2}$. Q_L was defined as the out-of-plane displacement of the diffuse scattering. The center of mass of the diffracted intensity was then determined as a function of laser delay [Fig. 2(b)]. We observe a transient decrease in the out-of-plane lattice constant (measured by Q_L) and the stripe domain period (measured by Q_r), followed by a long-lived increase on a timescale matching the monodomain room temperature response. The strong match between the timescales in both phases [Fig. 2(b)] indicates a mechanism independent of the intrinsic domain structure and rules out effects associated with photothermal desorption.

Based on the measurements described above, we propose the following two-step mechanism for the observed dynamics, driven by the displacement of electrons first against and then along the polarization direction (pointing out of the film) (Fig. 3). In the first step, the initial decrease in the ferroelectric tetragonality during the first 5 ps follows from a shift current, associated with a photoinduced, coherent shift of electrons away from the free surface [35,36]. This current, directed along the polarization direction, increases the charge density at the interfaces [37], giving rise to an increase in the depolarization field and an impulsive stress which leads to contraction of the lattice. We estimate this contribution by calculating the second-order nonlinear current in the applied light field, obtained by a first-principles calculation of the third-rank shift current tensor, in order to determine the photoinduced current density while the sample is illuminated [38]. For PTO (point group 4*mm*), the relevant tensor components have subscripts 31, 33, and 15; the 31 and 33 components represent the current parallel to the ferroelectric polarization; and their values depend on the light frequency and polarization [21,38]. Our calculation of the current direction is consistent with previous observations [13]. Quantitatively, we estimate surface charge densities of 5 $\mu C/cm^2$ for the fluences, light polarization and excitation wavelength used here. In the second step, after the light is turned off, the transient current reverses direction as the generated electrons and holes move in and screen the depolarization field, leading to an increase in the *c*-axis lattice parameter. This model is supported by several key observations:

(1) As noted before, concomitant with the changes in tetragonality, we observe dynamical changes in the stripe domain period, Λ, consistent with modification of the surface charge density and the depolarization field. Increases (decreases) in Λ reflect more complete (less complete) screening of the depolarization field by, for example, compensating ions, surface defects, or free charges [1,4,5,7]. These changes are analogous to the compensation effects observed in ferroelectrics with electrode structures [7].

(2) Corresponding measurements of PTO on DSO in the paraelectric phase [Fig. 4(a)], where the depolarization field vanishes due to the centrosymmetric unit cell, show negligible shifts in θ (<0.004°) during the first 20 ps. The centrosymmetry of the paraelectric phase also precludes second-order nonlinear optical responses such as shift currents, in agreement with our observations.

(3) In Fig. 4(b), the maximum observed *c*-axis lattice parameter for PTO on STO as a function of temperature is compared to the *c*-axis parameter without a depolarization field calculated from a Landau-Ginzburg-Devonshire (LGD) model, which predicts the equilibrium relationships between the polarization, *c*-axis parameter, internal field, and epitaxial strain seen by the PTO [9,39]. The fully compensated temperature-dependent polarization and resulting *c*-axis parameter were calculated by minimizing the bulk LGD free energy density under zero internal electric field (i.e., zero depolarization field) conditions [9], describing the case when the free carriers fully compensate the interfacial charge. This model considers the effect of epitaxial strain on the thermodynamic stability of ferroelectric PTO phases and accounts for the known temperature dependence of the STO lattice parameter [40]. Thermodynamic constants relevant to the ferroelectric properties of PTO were taken from literature values [41]. These numbers are in good agreement and are consistent with nearly complete screening of the internal field.

(4) As shown in Fig. 4(c), the induced strain at t = 100 ps saturates with increasing fluence. This observation is consistent with a free-carrier-induced screening of the internal field which saturates when the field is fully canceled [13,42,43] and is inconsistent with models associated with pyroelectric or other temperature-induced effects, which would result in *c*-axis lattice parameter changes in the opposite direction at long times and are not expected to saturate. We measure an absorption constant $\alpha_{PTO} = 1 \times 10^5$ cm^{-1} at λ = 400 nm by ellipsometry (in agreement

with our first-principles calculations of the absorption coefficient [38]), from which we estimate a carrier density $N \approx 10^{20}/\mathrm{cm}^3$ and a temperature jump of approximately 50 K [44] for the fluences used here.

The transient polarization change, ΔP_{eh}, associated with an electron-hole displacement Δz, is $\Delta P_{eh} = Nq\Delta z \approx 10\ \mu\mathrm{C/cm}^2$ for Δz comparable to the nanolayer thickness, consistent with the shift-current-induced modulation calculated above [45]. We scale the maximum observed Δc at $t > 10$ ps using the equilibrium electrostrictive response $\Delta c \sim |P|^2$ [39] to estimate the magnitude of the ferroelectric polarization increase, and obtain roughly 5 $\mu\mathrm{C/cm}^2$, a significant fraction of the initial polarization ($P_0 \approx 60\ \mu\mathrm{C/cm}^2$ [2]). Carrier motion in the internal field of the film is expected to develop on a timescale of roughly $\Delta z/(\mu E) \approx 5$ ps, using typical values for the carrier mobility ($\mu \approx 1\ \mathrm{cm}^2\ \mathrm{V}^{-1}\ \mathrm{s}^{-1}$) [46] and the internal field ($E \approx 500$ kV/cm) [39] in PTO. It is therefore delayed with respect to the shift current response, in agreement with our observations. At all temperatures, only small changes in the STO or DSO diffraction peaks are observed (not shown). Measurements using well-above-bandgap 266 nm pulses (not shown) show effects of similar magnitude at significantly lower fluences, of order 10 $\mu\mathrm{J/cm}^2$, consistent with the increased optical cross section at 266 nm. (We measure an absorption constant $\alpha_{\mathrm{PTO}} = 9 \times 10^5\ \mathrm{cm}^{-1}$ at $\lambda = 266$ nm.) This observation precludes optical rectification, which is expected to depend primarily on incident intensity, as a possible mechanism for these effects, consistent with previous work [22].

To further interpret Fig. 1, we model the strain evolution within the PTO as a response to an applied stress by the photogenerated currents [47]. The acoustic wave equation is solved for a thin film-substrate system for a time-dependent pressure described by the following equation:

$$\sigma(t) = H(t)\ \{\sigma_{SC} + \sigma_{DP}\ [1 - \exp(-t/\tau)]\} \quad \text{(Eq. 1)}$$

Here, $H(t)$ is the Heaviside step function and σ_{SC} represents an instantaneous stress associated with the shift-current-induced increase in the depolarization field. The subsequent tetragonality increase, ascribed to screening of the internal field by free carriers, leads to a slowly increasing stress, σ_{DP}, in the opposite direction, with a time constant τ determined by the carrier mobility. These stresses develop from the piezoelectric coupling between the lattice and the

internal field. Transient PTO (003) rocking curves resulting from the stress described by Eq. 1 are calculated using dynamical diffraction theory [48] and used to construct a predicted time scan like that of Fig. 1. As can be seen by comparison to the measured data (Fig. 3), this simple acoustic model provides an excellent description of the experimental results during the first tens of picoseconds. The best quantitative fitting is obtained for $\sigma_{DP}/\sigma_{SC} = -1.6$ and $\tau = 4$ ps, in good agreement with the estimates given above for the screening time.

The strong coupling between light, photocurrents, and atomic-scale degrees of freedom elucidated here determine the first steps in the processes that underlie the intrinsic photovoltaic response of ferroelectrics, and result from a current-driven modulation of the internal field within the thin film. This work provides new avenues for enhancing the functionality of ferroelectric devices on ultrafast timescales by a light-mediated coupling to their polarization. Further engineering of artificial ferroelectric structures and extensions of this work to light frequencies spanning the range from visible to terahertz may soon provide a technologically viable and facile pathway to ultrafast all-optical switching, addressing a key obstruction towards the goal of memory devices both written to and read out by light.

Acknowledgements

Portions of this research were carried out at the Linac Coherent Light Source (LCLS) at the SLAC National Accelerator Laboratory. LCLS is an Office of Science User Facility operated for the US Department of Energy (DOE) Office of Science by Stanford University. Use of the Advanced Photon Source, an Office of Science User Facility operated for the US DOE Office of Science by Argonne National Laboratory, was supported by the US DOE under contract DE-AC02-06CH11357. This work was supported by the US DOE, Basic Energy Sciences, Materials Sciences and Engineering Division (ultrafast x-ray studies of ferroelectrics, including M.J.H., P.H.F., G.B.S. and A.M.L.). S.M.Y. and A.M.R. were supported by the US DOE under contract DE-FG02-07ER46431. M.V., M.N., F.Q. and K.S.-T. acknowledge support by the *German Research Council* (SFB 616 *Energy dissipation at surfaces*). J.G. was supported by a DOE Office of Science graduate fellowship program. T.Q. and I.G. were supported by the Office of Naval Research under contract N00014-09-1-0157. J.L. acknowledges the support of the Swedish Science Council (VR).

References

[1] J. E. Spanier, A. M. Kolpak, J. J. Urban, I. Grinberg, L. Ouyang, W. S. Yun, A. M. Rappe, and H. Park, Nano Lett. **6**, 735–739 (2006).

[2] D. D. Fong, A. M. Kolpak, J. A. Eastman, S. K. Streiffer, P. H. Fuoss, G. B. Stephenson, C. Thompson, D. M. Kim, K. J. Choi, C. B. Eom, I. Grinberg, and A. M. Rappe, Phys. Rev. Lett. **96**, 127601 (2006).

[3] S. K. Streiffer, J. A. Eastman, D. D. Fong, C. Thompson, A. Munkholm, M. V. Ramana Murty, O. Auciello, G.-R. Bai, and G. B. Stephenson, Phys. Rev. Lett. **89**, 067601 (2002).

[4] S. Prosandeev and L. Bellaiche, Phys. Rev. B **75**, 172109 (2007).

[5] M. F. Chisholm, W. Luo, M. P. Oxley, S. T. Pantelides, and H. N. Lee, Phys. Rev. Lett. **105**, 197602 (2010).

[6] C. Lichtensteiger, J.-M. Triscone, J. Junquera, and P. Ghosez, Phys. Rev. Lett. **94**, 047603 (2005).

[7] I. P. Batra, P. Wurfel, and B. D. Silverman, Phys. Rev. B **8**, 3257–3265 (1973).

[8] D. D. Fong, G. B. Stephenson, S. K. Streiffer, J. A. Eastman, O. Auciello, P. H. Fuoss, and C. Thompson, Science **304**, 1650–1653 (2004).

[9] N. A. Pertsev, A. G. Zembilgotov, and A. K. Tagantsev, Phys. Rev. Lett. **80**, 1988–1991 (1998).

[10] G. Catalan, A. Janssens, G. Rispens, S. Csiszar, O. Seeck, G. Rijnders, D. H. A. Blank, and B. Noheda, Phys. Rev. Lett. **96**, 127602 (2006).

[11] N. Sai, A. M. Kolpak, and A. M. Rappe, Phys. Rev. B **72**, 020101 (2005).

[12] A. M. Glass, D. von der Linde, and T. J. Negran, Appl. Phys. Lett. **25**, 233–235 (1974).

[13] K. Uchino, Y. Miyazawa, and S. Nomura, Jpn. J. Appl. Phys. **21**, 1671–1674 (1982).

[14] V. M. Fridkin, Crystallogr. Rep. **46**, 654–658 (2001).

[15] M. Qin, K. Yao, and Y. C. Liang, Appl. Phys. Lett. **93**, 122904 (2008).

[16] T. Choi, S. Lee, Y. J. Choi, V. Kiryukhin, and S.-W. Cheong, Science **324**, 63–66 (2009).

[17] D. S. Rana, I. Kawayama, K. Mavani, K. Takahashi, H. Murakami, and M. Tonouchi, Adv. Mater. **21**, 2881–2885 (2009).

[18] S. Y. Yang, J. Seidel, S. J. Byrnes, P. Shafer, C.-H. Yang, M. D. Rossell, P. Yu, Y.-H. Chu, J. F. Scott, J. W. Ager III, L. W. Martin, and R. Ramesh, Nat. Nanotechnol. **5**, 143–147 (2010).

[19] W. Ji, K. Yao, and Y. C. Liang, Adv. Mater. **22**, 1763–1766 (2010).

[20] H. T. Yi, T. Choi, S. G. Choi, Y. S. Oh, and S.-W. Cheong, Adv. Mater. (2011).

[21] B. I. Sturman and V. M. Fridkin, *The Photovoltaic and Photorefractive Effects in Noncentrosymmetric Materials* (Gordon and Breach Science Publishers, Philadelphia, 1992).

[22] N. Laman, M. Bieler, and H. van Driel, J. Appl. Phys. **98**, 103507 (2005).

[23] T. Qi, Y. Shin, K. Yeh, K. Nelson, and A. M. Rappe, Phys. Rev. Lett. **102**, 247603 (2009).

[24] K. Istomin, V. Kotaidis, A. Plech, and Q. Kong, Appl. Phys. Lett. **90**, 022905 (2007).

[25] J. Larsson, P. Sondhauss, O. Synnergren, M. Harbst, P. A. Heimann, A. M. Lindenberg, and J. S. Wark, Chem. Phys. **299**, 157–161 (2004).

[26] B. Kundys, M. Viret, D. Colson, and D. O. Kundys, Nat. Mater. **9**, 803–805 (2010).

[27] C. v. Korff Schmising, M. Bargheer, M. Kiel, N. Zhavoronkov, M. Woerner, T. Elsaesser, I. Vrejoiu, D. Hesse, and M. Alexe, Phys. Rev. Lett. **98**, 257601 (2007).

[28] P. Emma, R. Akre, J. Arthur, R. Bionta, C. Bostedt, J. Bozek, A. Brachmann, P. Bucksbaum, R. Coffee, F.-J. Decker, Y. Ding, D. Dowell, S. Edstrom, A. Fisher, J. Frisch, S. Gilevich, J. Hastings, G. Hays, P. Hering, Z. Huang, R. Iverson, H. Loos, M. Messerschmidt, A. Miahnahri, S. Moeller, H.-D. Nuhn, G. Pile, D. Ratner, J. Rzepiela, D. Schultz, T. Smith, P.

Stefan, H. Tompkins, J. Turner, J. Welch, W. White, J. Wu, G. Yocky, and J. Galayda, Nat. Photonics **4**, 641–647 (2010).

[29] J. M. Glownia, J. Cryan, J. Andreasson, A. Belkacem, N. Berrah, C. I. Blaga, C. Bostedt, J. Bozek, L. F. DiMauro, L. Fang, J. Frisch, O. Gessner, M. Guhr, J. Hajdu, M. P. Hertlein, M. Hoener, G. Huang, O. Kornilov, J. P. Marangos, A. M. March, B. K. McFarland, H. Merdji, V. S. Petrovic, C. Raman, D. Ray, D. A. Reis, M. Trigo, J. L. White, W. White, R. Wilcox, L. Young, R. N. Coffee, and P. H. Bucksbaum, Opt. Express **18**, 17620–17630 (2010).

[30] M. V. Ramana Murty, S. K. Streiffer, G. B. Stephenson, J. A. Eastman, G.-R. Bai, A. Munkholm, O. Auciello, and C. Thompson, Appl. Phys. Lett. 1809–1811 (2002).

[31] G. Koster, B. L. Kropman, G. J. H. M. Rijnders, D. H. A. Blank, and H. Rogalla, Appl. Phys. Lett. **73**, 2920–2922 (1998).

[32] J. E. Kleibeuker, G. Koster, W. Siemons, D. Dubbink, B. Kuiper, J. L. Blok, C.-H. Yang, J. Ravichandran, R. Ramesh, J. E. ten Elshof, D. H. A. Blank, and G. Rijnders, Adv. Funct. Mater. **20**, 3490–3496 (2010).

[33] D. D. Fong, C. Cionca, Y. Yacoby, G. B. Stephenson, J. A. Eastman, P. H. Fuoss, S. Streiffer, C. Thompson, R. Clarke, R. Pindak, and E. Stern, Phys. Rev. B **71**, (2005).

[34] Z. Li, M. Grimsditch, X. Xu, and S.-K. Chan, Ferroelectrics **141**, 313–325 (1993).

[35] D. Cote, N. Laman, and H. van Driel, Appl. Phys. Lett. **80**, 905–907 (2002).

[36] F. Nastos and J. E. Sipe, Phys. Rev. B **82**, 235204 (2010).

[37] A. V. Ruzhnikov, *Electrons, Phonons and Ferroelectrics* (Herzen University Press, Leningrad, 1979), pp. 49–51.

[38] S. M. Young and A. M. Rappe (in review).

[39] M. J. Highland, T. T. Fister, M.-I. Richard, D. D. Fong, P. H. Fuoss, C. Thompson, J. A. Eastman, S. K. Streiffer, and G. B. Stephenson, Phys. Rev. Lett. **105**, 167601 (2010).

[40] Y. S. Touloukian, *Thermal Expansion—Nonmetallic Solids* (IFI/Plenum, New York, 1977).

[41] M. J. Haun, Z. Q. Zhuang, E. Furman, S. J. Jang, and L. E. Cross, Ferroelectrics **99**, 45–54 (1989).

[42] J. T. Darrow, X.-C. Zhang, and D. H. Auston, Appl. Phys. Lett. **58**, 25–27 (1990).

[43] Y.-C. Wen, L.-C. Chou, H.-H. Lin, V. Gusev, K.-H. Lin, and C.-K. Sun, Appl. Phys. Lett. **90**, 172102 (2007).

[44] G. A. Rossetti and N. Maffei, J. Phys.: Condens. Matter **17**, 3953–3963 (2005).

[45] T. Dekorsy, T. Pfeifer, W. Kütt, and H. Kurz, Phys. Rev. B **47**, 3842–3849 (1993).

[46] J. F. Scott, Science **315**, 954–959 (2007).

[47] M. Nicoul, U. Shymanovich, A. Tarasevitch, D. von der Linde, and K. Sokolowski-Tinten, Appl. Phys. Lett. **98**, 191902 (2011).

[48] D. A. Reis and A. M. Lindenberg, in *Topics in Applied Physics: Light Scattering in Solids IX*, edited by M. Cardona and R. Merlin (Springer, Berlin, 2007), pp. 371–422.

Figures

FIG. 1. Evolution of the tetragonality of PTO on STO in the monodomain phase. (a) Time scans on the low- and high-angle sides of the PTO (003) rocking curve at room temperature (incident fluence = 5 mJ/cm^2). We observe an acoustically limited high-Q shift, followed by a long-lived low-Q shift. (b) Rocking curve scans at various time delays denoted in (a). (c) Long-range time scan on the low-angle side of PTO (004) at 350° C (incident fluence = 5 mJ/cm^2). The observed low-Q shift decays on single-nanosecond timescales.

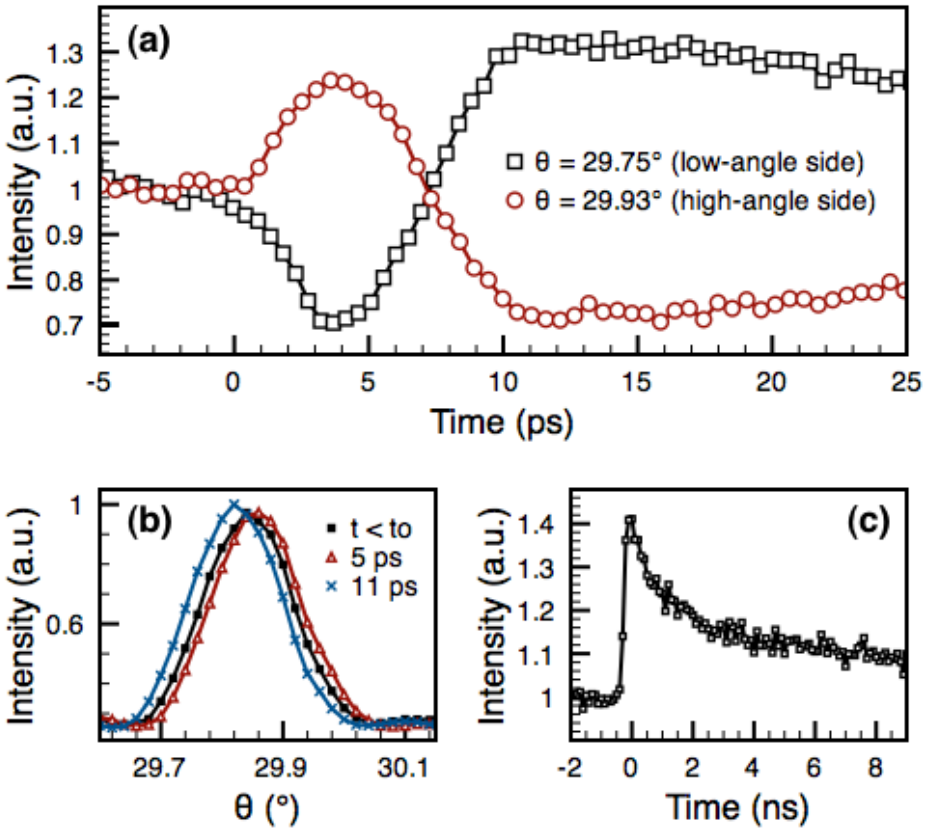

FIG. 2. Stripe domain phase response at 535° C. (a) Area detector images of PTO (003) at 535° C for several time delays (incident fluence = 5 mJ/cm^2), corrected such that the angle of the detector plane is normal to the *L*-axis in reciprocal space. (b) Time evolution of Q_L and Q_r, extracted from area detector images of PTO (003). Q_L is the position of the diffuse scattering ring along the *L*-axis and Q_r is the radius of the diffuse ring.

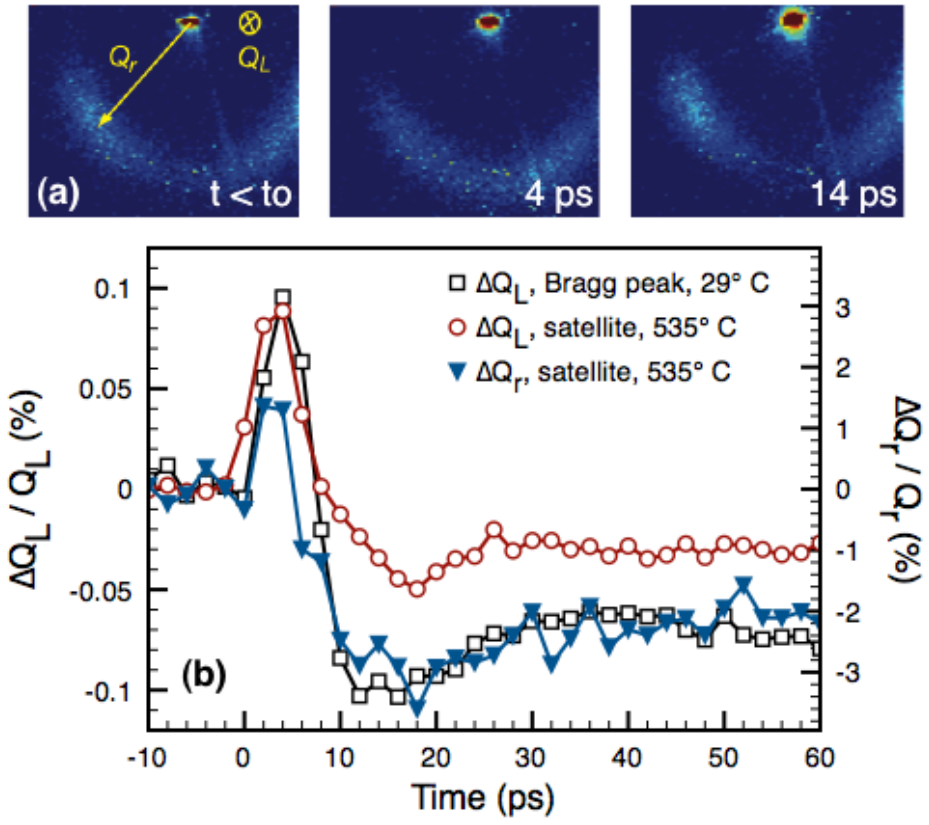

FIG. 3. Schematic of unit cell response. At t = 5 ps, the c-axis lattice parameter reaches a minimum due to the piezoelectric response to the increase in the depolarization field, E_d, induced by the shift current. At t > 10 ps, carriers have moved to screen the depolarization field, driving a long-lived increase in tetragonality. Time scans from Fig. 1 are fit by modeling the out-of-plane strain of PTO as a response to the time-dependent stress profile given in the inset (see Eq. 1). Vertical lines are guides to the eye.

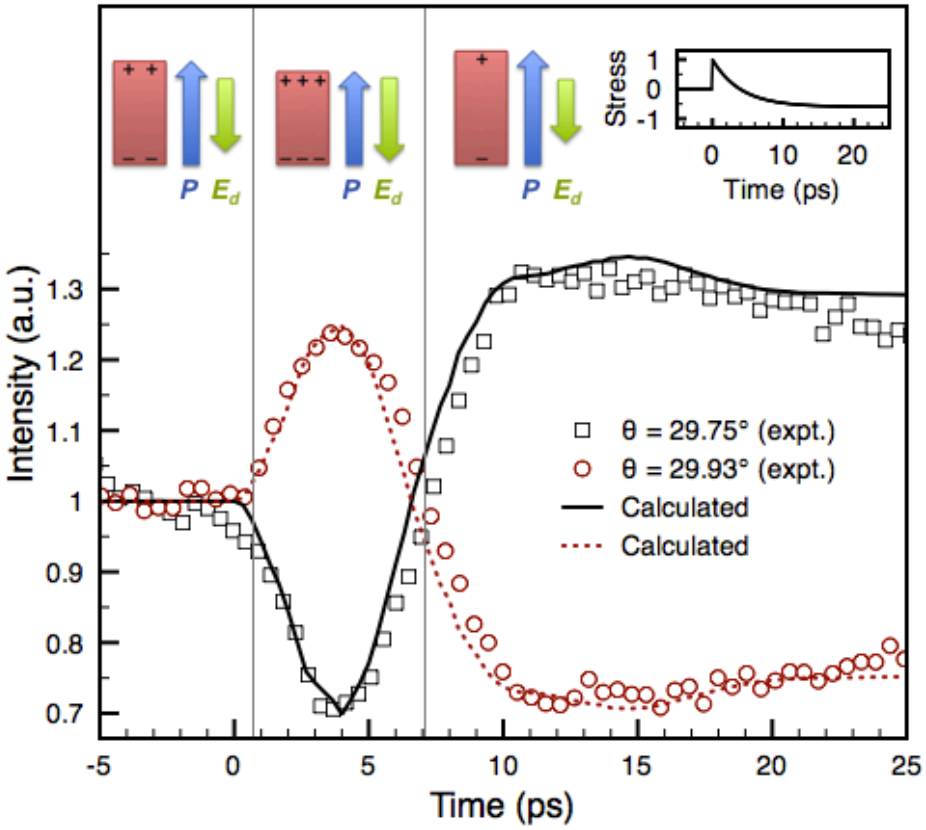

FIG. 4. Role of depolarization field in photovoltaic response. (a) PTO (003) on DSO in the paraelectric phase at 479° C, slightly above T_C (incident fluence = 5 mJ/cm^2). Only small θ shifts are seen due to the centrosymmetric, paraelectric unit cell. (b) LGD theory calculation, comparing the observed *c*-axis lattice parameter of PTO on STO at $t < t_0$ and t = 100 ps (incident fluence = 4 mJ/cm^2) to the predicted zero-field *c*-axis parameter. (c) Strain in the *c*-axis parameter of monodomain PTO on STO at 550° C as a function of fluence, measured at t = 100 ps. Saturation behavior in the maximum drivable strain is seen.